Dendrochronologia 50 (2018) 10–22

Contents lists available at ScienceDirect

Dendrochronologia

journal homepage: www.elsevier.com/locate/dendro

Blue intensity from a tropical conifer's annual rings for climate reconstruction: An ecophysiological perspective

Brendan M. Buckley[a,*], Kyle G. Hansen[a,b], Kevin L. Griffin[a,c], Stephanie Schmiege[c], Rose Oelkers[a,b], Rosanne D. D'Arrigo[a], Daniel K. Stahle[a], Nicole Davi[a,b], Tran Quoc Trung Nguyen[d], Canh Nam Le[e], Rob J.S. Wilson[a,f]

[a] Lamont-Doherty Earth Observatory of Columbia University, NY, USA
[b] William Paterson University, Wayne, NJ, USA
[c] Department of Ecology, Evolution and Environmental Biology, Columbia University, NY, USA
[d] Southern Institute of Ecology, Vietnam Academy of Science and Technology, HCMC, Vietnam
[e] Forest Science Institute of Central Highlands and South of Central Viet Nam, Dalat City, Lam Dong Province, Vietnam
[f] School of Earth and Environmental Sciences, University of St Andrews, Scotland, UK

ARTICLE INFO

Keywords:
Blue intensity
Tropical dendrochronology
Fokienia hodginsii
Vietnam
Dendroclimatology
Monsoon climate

ABSTRACT

We developed Blue Intensity (BI) measurements from the crossdated ring sequences of *Fokienia hodginsii* (of the family Cupressaceae) from central Vietnam. BI has been utilized primarily as an indirect proxy measurement of latewood (LW) density of conifers (i.e., LWBI) from high latitude, temperature-limited boreal forests. As such, BI closely approximates maximum latewood density (MXD) measurements made from soft x-ray. The less commonly used earlywood (EW) BI (EWBI) represents the minimum density of EW and is influenced by the lighter pixels from the vacuoles or lumens of cells. The correlation of our BI measurements with climate, strongest for EWBI, rivals that for total ring width (RW), and we demonstrate that it can be successfully employed as an independent predictor for reconstruction models. EWBI exhibits robust spatial correlations with winter and spring land temperature, sea surface temperature (SST) over the regional domain of ENSO, and the Standardized Precipitation Evapotranspiration Index (SPEI) over Indochina. However, in order to mitigate the effects of color changes at the heartwood – sapwood boundary we calculated ΔBI (EWBI-LWBI), and it too exhibits a significant ($p < 0.05$), temporally stable response to prior autumn (Oct-Nov) rainfall and winter (December to April) dry season temperature. We interpret this response as reflecting a potential cavitation defense by reducing lumen diameter as a means to safeguard hydraulic conductivity in the stem, and to prevent the xylem from imploding due to negative pressure. This study has wide implications for the further use of BI from the global tropics, though it is unclear how many tropical tree species will be appropriate for use. It seems very likely that other wood anatomical measurements can be combined with BI and RW for climate reconstruction.

1. Introduction

In dendroclimatology, the maximum latewood density (MXD, expressed as grams/cm^3) of tree rings is a parameter measured directly by soft X-ray of carefully prepared thin sections of wood (Schweingruber, 2012). MXD, most commonly measured from temperature-limited conifers of the Northern Hemisphere high latitudes, often expresses a stronger correlation with current growing season temperature than does total ring width (RW). This is in part because RW of conifers exhibits a strong autocorrelation that reflects the carry-over effects from the previous year's growth that are often the result of non-climatic signals related to stand dynamics and endogenous disturbances (Cook and Kairiukstis, 1990; Fritts, 1976). Conversely, the autocorrelation of MXD is much more closely aligned to what is exhibited by temperature data (Briffa et al., 2002; Rydval et al., 2014), owing to a more direct current-season response to temperature than is expressed for RW. Therefore MXD is more reflective of the secondary process of cell lignification of the latewood, a process that is largely controlled by late growing season temperature (Mork, 1960). Accordingly, including MXD with RW for reconstruction of growing season temperature often increases the skill and spectral fidelity of reconstruction models (e.g., D'Arrigo et al., 2003; Wilson and Luckman, 2003; Wilson et al., 2016).

Blue reflectance or blue intensity (BI) is an image analysis based measurement that is interpreted as a proxy for the density of tree rings

* Corresponding author.
E-mail address: bmb@ldeo.columbia.edu (B.M. Buckley).

https://doi.org/10.1016/j.dendro.2018.04.003
Received 7 August 2017; Received in revised form 3 March 2018; Accepted 13 April 2018
Available online 22 April 2018

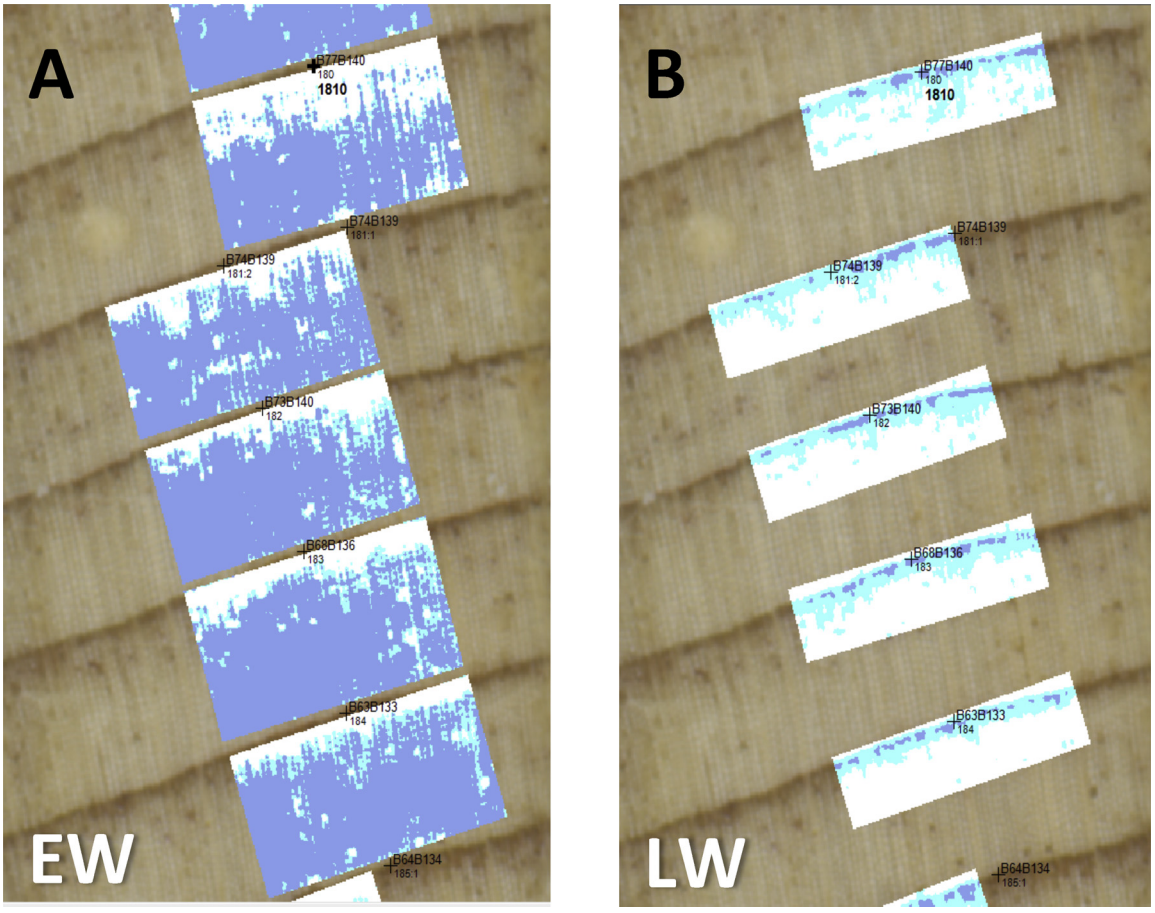

Fig. 1. CooRecorder image analysis software collects BI and RW measurements for each annual ring. For EW (A) all pixels in the highlighted box are sorted by dark and light wood (white and blue, respectively), and the whitest 85% of pixels are measured (dark blue). For LW (B) measurements are taken from the 15% of the darkest pixels (dark blue). To measure ΔBI the LW measurements are subtracted directly from the EW measurement, using an average of 100% of the pixels (For interpretation of the references to colour in this figure legend, the reader is referred to the web version of this article).

(Campbell et al., 2007). The procedure is theoretically based upon the compound lignin's propensity to absorb ultraviolet light more readily than other wood structural components (Fukazawa, 1992). It is likely, however, that BI also reflects cellulose and hemi-cellulose, both of which are companion constituents of lignin in tracheid cell walls (Vincent, 1999; Yan et al., 2004). The higher the degree of reflected blue light, the less dense (i.e., less lignified) the wood and vice versa (Fig. 1). The understanding of this property dates back to Lange (1954) who utilized UV photomicrographs to measure the lignin content in the latewood of spruce. However it was only recently that Gindl et al. (2000) more formally made the connection between lignin content (density), as measured through UV photomicrographs, and temperature. BI from the growth rings of high-latitude/altitude trees has been shown to serve as an indirect proxy of wood density and therefore temperature of the late growing season. Consequently BI has been mostly used for high latitude/altitude conifer species where temperature has been shown to exert the greatest control on growth relative to other climate parameters (Björklund et al., 2014; 2015; Campbell et al., 2007; Dolgova, 2016; Rydval et al., 2014; 2017a; 2017b; Wilson et al., 2014; 2017a).

Both the new method of BI and the preceding work on MXD are predicated on the relationship between temperature and lignin content of the tracheid cells of conifers, and are most commonly applied to the latewood. Within a given species' optimal range, cooler temperatures inhibit and warmer temperatures enhance photosynthesis and, consequently, lignification. At high-latitude/altitude sites, cooler than average growing season temperature is correlated with less lignin allocated to tracheid cell walls, resulting in low-density rings for anomalously cool years known as "light rings" (e.g., Filion et al., 1986; Gindl, 1999; Szeicz, 1996; Waito et al., 2013). Similarly, hemispheric cooling caused by years of large volcanic eruptions may result in extreme reduction in the density of growth rings across a broad region (e.g., D'Arrigo et al., 2013; Esper et al., 2013, 2015; Gindl et al., 2000; Jacoby et al., 1999; Szeicz, 1996). Since lignification is a process secondary to the formation of the cells (i.e., cells are formed first and then lignified – *sensu* Mork, 1960) an abrupt reduction in growing season temperature below optimum levels can result not only in light rings, but often in "frost rings" where tracheid cells deficient in lignin rupture in response to freezing of their internal water (Fig. 2). Conversely, a warmer than average end to the growth season allows for a greater degree of lignification and an increase in the density of the latewood.

Given the discussion above, it stands to reason that BI would afford the same advantages over RW as does MXD, and for a fraction of the cost in time and money. Wilson et al. (2014) show that BI typically requires a larger sample size than MXD to improve signal strength, but due to the comparatively low cost of generating BI this is usually not a concern. Potential limitations remain, however, such as the effect of color changes at the heartwood-sapwood boundary for many species that can impart trend to data that may have nothing to do with a systematic climate related change in density (Björklund et al., 2014). Discoloration may also occur as the result of physiological response to a variety of non-climatic factors such as infusion of resin (and other compounds) near the site of an injury. Hence, trees with a particularly high contrast of wood color due to high resin content may exhibit either an abrupt or slow change in reflectance values that is not climatic in origin, and which distorts the BI time series (Fig. 3). It is currently

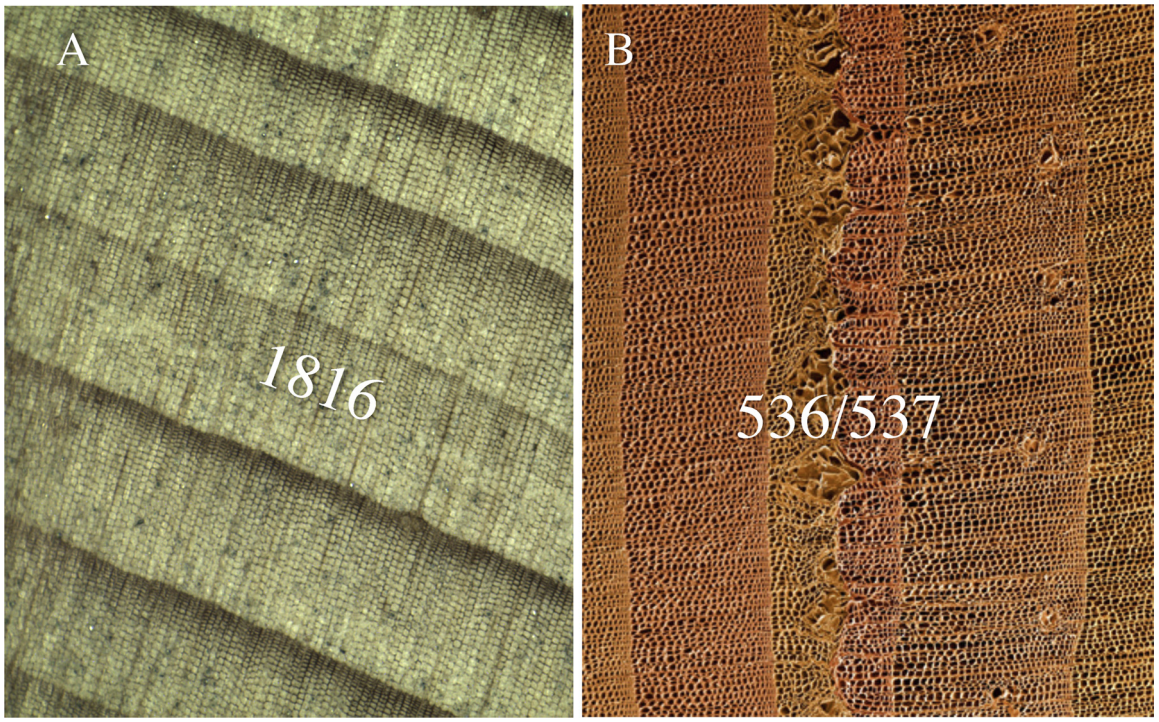

Fig. 2. In (A) a light density ring found in white spruce from near the northern tree line in Labrador, Canada. The light density latewood is from the year 1816, following the 1815 eruption of Tambora in Indonesia (one of the most powerful eruptions in recorded history). A frost ring (B) in Siberian pine from Mongolia for the year 536 C.E., the result of drastic cooling that froze sap water in the cells during the growing season and ruptured cell walls (SEM photomicrograph courtesy of Dee Breger). Evidence for this abrupt climate change points to a massive eruption of the volcanic precursor of Krakatoa (D'Arrigo et al., 2001).

unclear to what extent the BI method can be applied away from high latitude/altitude tree line sites that are known for their temperature sensitivity. Up until this current study, the BI methodology has not been applied in tropical regions where precipitation sensitivity dominates the tree ring response.

There is a dearth of research on the influence of hydroclimate on the density of tree rings, as well as on the complexities of how climate and secondary cellular processes like lignification are connected through tree physiology. Several studies have linked increased wood density to drought (e.g., Hoffmann et al., 2011; Xiao et al., 2014; Starheim et al., 2013), and Hacke et al. (2001) demonstrate a clear relationship between wood density and the prevention of xylem implosion for drought tolerant trees. However, no prior work that we could find made a connection between the density of tropical tree rings and climate,

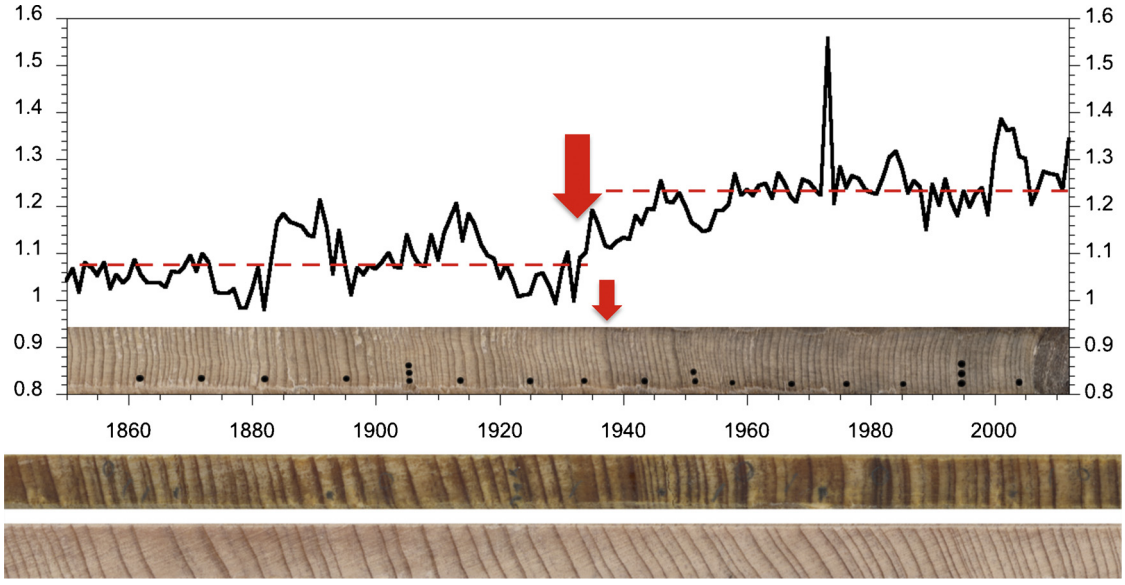

Fig. 3. Here we plot the inverted EWBI time series for core QNFH59B where two distinct periods result from a color change in the mid 1930s indicated by the red arrows. The mean EWBI for the period 1850–1935 = 1.0767, and then changes to a mean of 1.2329 for the period 1935–2013. This abrupt change is entirely the result of the color change and not a real change in density (the inversion results in an increased step where the raw BI would reflect a decrease). The calculation of ΔBI, as described in the text, attempts to negate this effect (For interpretation of the references to colour in this figure legend, the reader is referred to the web version of this article).

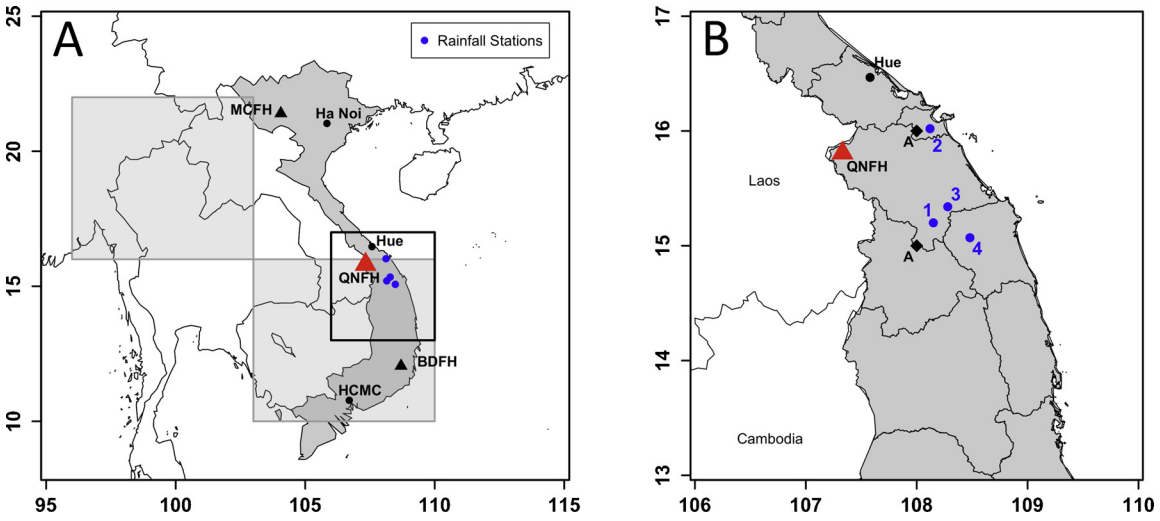

Fig. 4. The study location at Tay Giang Forest Protection (QNFH) area in Quang Nam province (red triangle in both maps): in (A) a regional overview and (B) a close up of the black box in (A). The blue dots denote a series of rainfall station data that were used to develop a regional rainfall record. The locations of two other published records of *Fokienia hodginsii* ring width data are indicated by the black triangles (A) at MCFH (Sano et al., 2009) and at BDFH (Buckley et al., 2010). The two gray boxes denote the areal extent of SPEI data used by Buckley et al. (2017) for reconstruction from the QNFH ring width data. (For interpretation of the references to colour in this figure legend, the reader is referred to the web version of this article).

particularly through the implementation of BI methodology. With this paper we present the first use of BI from within the tropics from crossdated core samples from the Vietnamese cypress *Fokienia hodginsii* (family Cupressaceae). The cores come from the Tay Giang Protection Forest in Quang Nam Province in central Vietnam (Fig. 4), from a collection published by Buckley et al. (2017). With this paper we present the first evidence that BI can be applied to tropical conifers and used for the reconstruction of climate. We first compare the results of BI with RW as a predictor for April SPEI, the reconstruction of which was published by Buckley et al. (2017) from these same samples based on RW alone. We then explore linkages between BI and factors related to the broader regional climate. In this case the reflection of climate resides most strongly within the earlywood (EW) portion of growth rather than the latewood (LW), and is most finely tuned to temperature during the winter dry season.

2. Materials and methods

2.1. Site description

As described in Buckley et al. (2017) the *Fokienia hodginsii* (Po Mu) trees used for this study come from the Tay Giang Protected Forest in Central Vietnam's Quang Nam Province, growing on variable terrain between 1000 and 1,500 m above mean sea level. These trees were part of a virtually undisturbed mixed evergreen broadleaved-coniferous forest that grows on a dense humus layer over a very porous limestone substrate. Five conifer species are found at this site including Po Mu, which along with the two Podocarps *Dacrycarpus imbricatus* and *Dacrydium elatum,* are canopy emergent. Two other Podocarps, *Nageia wallichiana* and *Podocarpus neriifolius,* play a less dominant role in the mid-canopy and the understory. Multiple broadleaf species, most notably from the canopy dominant families of Magnoliaceae, Fagaceae and Theaceae, are also present at the study location (see Buckley et al., 2017 for further detail).

The region of Central Vietnam that surrounds the study location experiences its seasonal rainfall peak in autumn (October–December), rather than summer (June to September). A study by Li et al. (2015) revealed a pronounced decadal oscillation of autumn precipitation over Central Vietnam within the 8–11 year frequency band. This oscillation appears to be modulated by the East Pacific–North Pacific (EP–NP) teleconnection, in conjunction with ENSO-like lower frequency variability. Positive SST anomalies in the South China Sea are associated with the negative phase of the EP–NP pattern, and these anomalies induce low-level convergence, enhance convection, and increase precipitation over Central Vietnam. This circulation feature is embedded in the large-scale circulation associated with SST anomalies across the Pacific Ocean, where cooling in the Eastern and Central tropical Pacific is flanked by warm anomalies in the North and South Pacific and a warm Western Pacific Ocean. The positive phase of the EP–NP is exemplified by opposing SST and circulation anomalies that reduce rainfall over Central Vietnam (Li et al., 2015). Warming SST and enhanced southerly low-level winds coincide with increased rainfall and tropical cyclones, and are part of a hemispheric-scale change in the general circulation in the form of a La Niña-like SST anomaly and a strengthened Walker circulation branch that ascends near Vietnam and the far-western Pacific (Wang et al., 2014).

2.2. Core preparation

We selected 29 core samples from 20 *Fokienia hodginsii* trees from the QNFH core collection of Buckley et al. (2017) that was based upon 71 cores from 39 trees. Each of these core samples was crossdated and measured for RW prior to this study, hence all missing rings and false rings were accounted for. Selection criteria for the current study focused on those cores that exhibited the highest mean series intercorrelation (MSI), the longest segment length, and the fewest missing rings. Since this subset has substantially fewer samples than the original, we compare the two RW records in Fig. 5 in order to demonstrate that the reduction in sample depth does not significantly alter the original QNFH growth index ($r = 0.93$ for the two versions of the record). Most importantly only minor departures in low-frequency variability are evident between the two records. For comparison purposes a full tabulation of the basic statistics for RW and BI parameters (EW, LW and ΔBI) from this subset of cores can be found in Table 1, while the four tree-ring parameter time series developed for this paper are plotted in Fig. 6. Prior to measuring BI, surficial pencil marks related to the crossdating procedure were removed from all cores before immersion in a solution of 99.5% acetone for 90 h. The acetone bath procedure is necessary to remove resin and diminish potential color transitions related to the heartwood-sapwood boundary (Fig. 3). After removal from the acetone the cores were air dried and re-sanded with micromesh abrasives in order to produce the best possible surface for image

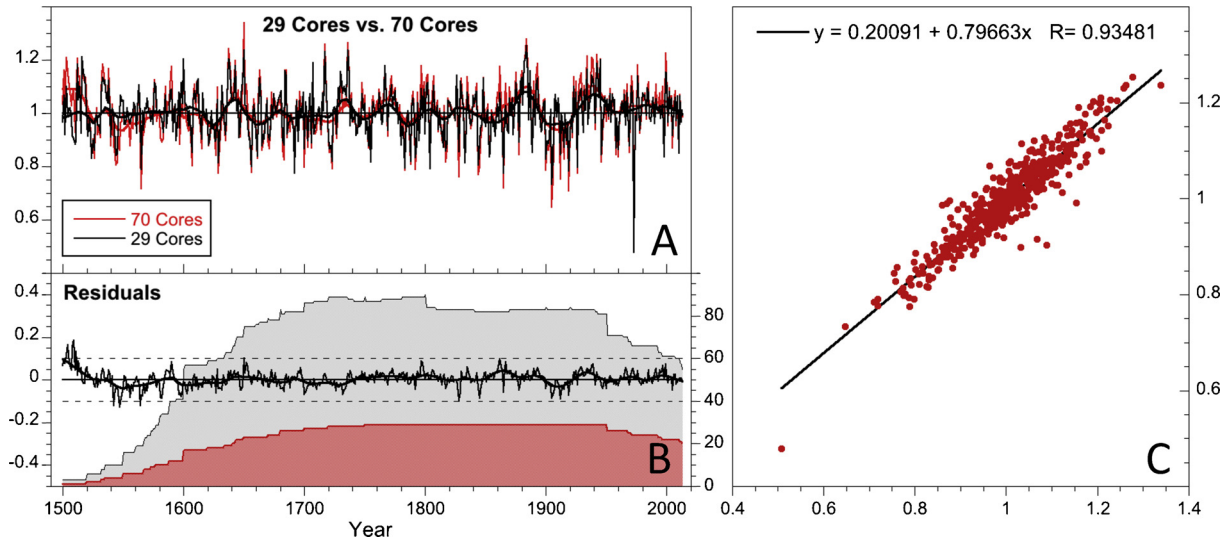

Fig. 5. Comparison plot of the two versions of the QNFH RW index (A) with original Buckley et al. (2017) 70-core version in red and our 29-core version in black. The residuals of the two records are shown in (B) along with sample depth as the gray and red shaded areas (right y axis), and the dashed lines representing 0.1 mm to either side of zero. Panel (C) shows a scatterplot of the two series that correlate at 0.93, indicating how little is lost with the reduction in sample size for our study (For interpretation of the references to colour in this figure legend, the reader is referred to the web version of this article).

Table 1
Basic statistics from the two versions of our QNFH tree ring record: a 70-core collection used by Buckley et al. (2017) for a reconstruction of April SPEI, and the 29-core subset of these cores presented in the current paper. The first and last year of record is included along with values for mean series intercorrelation (MSI), mean sensitivity (Mean Sens.) and serial autocorrelation (Auto Corr.) as described in the text.

Series	First year	Last Year	MSI	Mean Sens	Auto Corr.
RW - 70 Core	1347	2013	0.526	0.302	0.638
RW - 29 Core	1500	2013	0.554	0.309	0.636
ΔBI	1508	2013	0.358	0.141	0.424
EWBI	1508	2013	0.332	0.058	0.493
LWBI	1508	2013	0.142	0.047	0.396

analysis using an Epson Perfection V850 Pro model scanner and Silverfast software at 3200 dpi resolution. Prior to imaging, we calibrated the scanner using a Monaco reflective MONR2015:03-01 IT8.7/2 calibration target. We then used the image analysis software CooRecorder 8.1 (Larsson, 2016) to measure RW, and BI from the latewood (LWBI) and earlywood (EWBI) portions of each ring.

2.3. Measuring Blue intensity from scanned images

The high-resolution scanned images from each crossdated core were first imported into CooRecorder, and then a box was selected over the latewood of each ring. Maximum parameters were set to 200 pixels wide, and 50 pixels deep (see Fig. 1). Once each box was defined, only the blue component of the reflected light was analyzed. Within each box all pixels were ranked in order of the measured amount of blue on a color-depth scale that is based on an 8-bit encoding where every channel is resolved with 256 possible values that range from 1–256. A value of 1 denotes complete absorption of visible blue light and high density (i.e., maximum lignin content), while a value of 256 indicates that all blue light is reflected and the density is low (minimum lignin content). A value of 0 was used in the case of an absent ring. Of the blue pixels in the defined box for LW (i.e., those pixels that register as having lignin), we used the mean pixel values of the lowest 15th percentile (i.e., those pixels at the low end of the scale with the highest degree of lignification), and this was used as the preliminary measurement for LWBI – the putative BI analogue of MXD. We then defined a box over the earlywood portion of each ring, with parameters set to 200 pixels wide and 500 pixels deep. All EW pixels were again ranked, but we now averaged the highest 85% of blue intensity values (i.e., those pixels at the 256 end of the color depth scale that represent the least amount of lignification) – the BI analogue of minimum earlywood density. It should be noted that in practice the actual width and depth of the boxes selected for both LW and EW may vary, and the box dimensions will scale smaller when the box depth dimension is larger than the ring's width, thereby ensuring there is no overlap with adjacent rings.

Preliminary BI data is essentially inversely correlated to density, since dense cell walls express lower reflectance as more blue light is absorbed. We therefore interpret BI as reflecting cell wall density through the amount of lignin in the cells, though it is possible that other anatomical features are responsible for BI variability as well, particularly for EWBI, such as the lumen diameter as noted previously. Typically a MXD time series exhibits a decreasing trend with increasing age, while for BI trend increases with age. The traditional methods for detrending time series for dendrochronology within the program ARSTAN (Cook, 1985) does not allow positive-linear-only detrending as a standard option, hence BI measurements are inverted to accommodate this detrending option (Björklund et al., 2014; 2015). Ostensibly inversion allows BI values to be more easily comparable to MXD, but it is perhaps best not to equate the two measurements until further research confirms the connection of BI to wood anatomy. Regardless, for consistency with other papers we inverted our data for EWBI and LWBI (see Rydval et al., 2014) by multiplying each value by -1 before adding the constant 2.56 to eliminate any negative values. This constant was used because the values are recorded in decimal form with the max color intensity set at 2.56 (i.e., 256 on the color model described above). Care was taken to ensure that rings denoted as absent for any series (hence given a value of zero) were not corrupted by this procedure, and still retain their original value of zero.

The Vietnamese cypress used for this study is a tropical conifer that is known to have a high resin content that often imparts a marked change in color at the heartwood/sapwood boundary (see Fig. 3). In order to account for color changes from each core that were not adequately removed by the acetone bath, ΔBI was calculated by subtracting each non-inverted LWBI value from its corresponding year's non-inverted EWBI value (Björklund et al., 2014). In their paper, Björklund et al. (2014) presented ΔBI for *Pinus sylvestris* cores from a site in Sweden that seemed to successfully account for the heartwood/

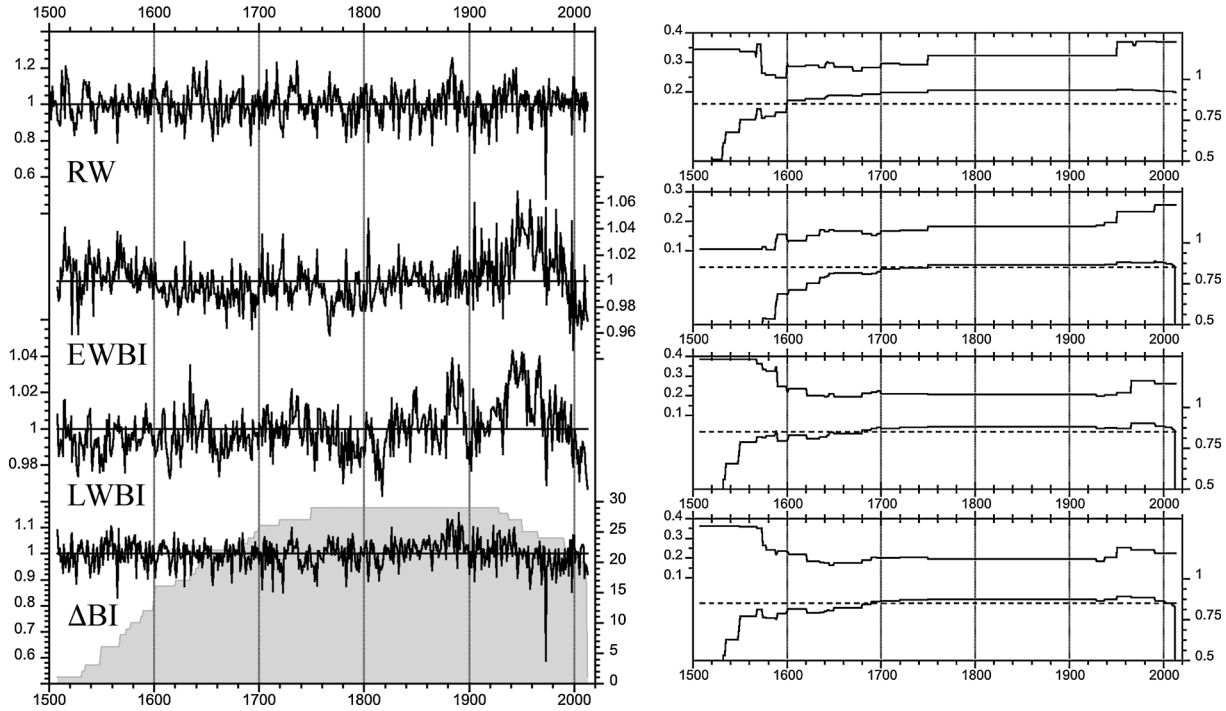

Fig. 6. Stacked plot of the 4 time series produced for this study (left) with their corresponding EPS and Rbar statistics (right). From top to bottom the series are RW, EWBI, LWBI and ΔBI. The gray shaded area on the left (bottom) indicates the sample depth through time.

sapwood color change. These authors emphasized, however, that ΔBI may have limited application when the correlation between EWBI and LWBI is high, as this may remove signals related to climate, provided that there is climate related common signal. As of this writing, the use of ΔBI is a relatively new method and has been only used for dendroclimatic reconstruction outside Scandinavia using mountain hemlock (*Tsuga mertensiana*) sites along the Gulf of Alaska (Wilson et al., 2017b). This study is the very first comparative study of EW, LW and BI metrics in order to assess the relative merits of each of the metrics in understudied and challenging tropical conifers.

2.4. Standardizing growth indices

It is common practice in dendrochronology to standardize growth indices in order to equalize variance through time and to account for what is commonly referred to as the biological growth trend (e.g., Fritts, 1976; Cook, 1985). Standardization also allows for comparing time series with distinctly different growth rates (i.e., mean and standard deviation), whether accounting for the overall growth rate of each tree or the systematic changes in mean and variance throughout each tree's lifespan (see Cook and Peters, 1997). For this study we used the same methodology that Buckley et al. (2017) used for standardizing the RW record; Signal Free standardization as developed by Melvin and Briffa (2008, 2014) and Briffa and Melvin (2011). For this purpose we used the program RCSig, a freeware program developed at the Lamont-Doherty Earth Observatory (http://www.ldeo.columbia.edu/tree-ring-laboratory/resources/software), and based on the commonly used program ARSTAN (Cook, 1985). RCSig allows for detrending individual series using methods routinely available in ARSTAN, but within a signal-free framework (see Melvin et al., 2007). For trees growing in forests with high species diversity, complex forest dynamics and high rainfall (such as the study location), the within-forest dynamics may exert influence over ring-width patterns (including BI) that competes with climate. Therefore, stochastic methods of detrending are more appropriate than deterministic detrending techniques such as negative exponential or linear regression models (Cook and Kairiukstis, 1990).

Using a signal-free framework reduces potential end effect biases that can occur during detrending by removing the common forcing signal within each series (Melvin et al., 2007). Accordingly, individual series in our study were detrended using an age-dependent smoothing spline, and the bi-weight robust mean for developing growth indices in order to reduce the effects of outliers (Cook and Kairiukstis, 1990). To quantify the signal strength of our record through time we calculated two common statistics, the RBAR and the Expressed Population Signal or EPS (Wigley et al., 1984). The RBAR metric analyzes the common signal between the available bivariate pairs for any one time, and while its value will not change with N, it will be biased as the relative number of within-tree correlations increases compared to between-tree correlations. In contrast EPS is sensitive to changes in N, as it estimates the hypothetical squared correlation value between the sample chronology and the theoretical infinitely replicated chronology. EPS values that exceed 0.85 are generally considered to demonstrate an acceptable level of common signal fidelity, though there is no actual significance test (Wigley et al., 1984). Both EPS and RBAR were calculated for successive 51-year windows and are presented along with each of our time series in Fig. 6.

2.5. Climate data and analyses

We used the online resource KNMI Climate Explorer (Trouet and Van Oldenborgh, 2013) to assess the spatial correlations of our RW and BI time series with various features of the global climate (e.g., sea surface temperature, maximum temperature over land, standardized precipitation evapotranspiration index, etc.). In addition, we used several freeware programs developed at the Lamont-Doherty Earth Observatory Tree Ring Lab, such as program PCReg that was used for climate response modeling and reconstruction. For comparison purposes, we used the same climate datasets as Buckley et al. (2017), but also shown in Fig. 7 are the monthly correlations with a local rainfall mean and variance adjusted composite of 4 stations from the Quang Nam region (locations shown in Fig. 4) that was not available to us prior to this study. Additional data included gridpoints extracted from the APHRODITE (Yatagai et al., 2012), and CRU TS3.24.01 (Harris and Jones, 2017) temperature and precipitation networks, the Berkeley

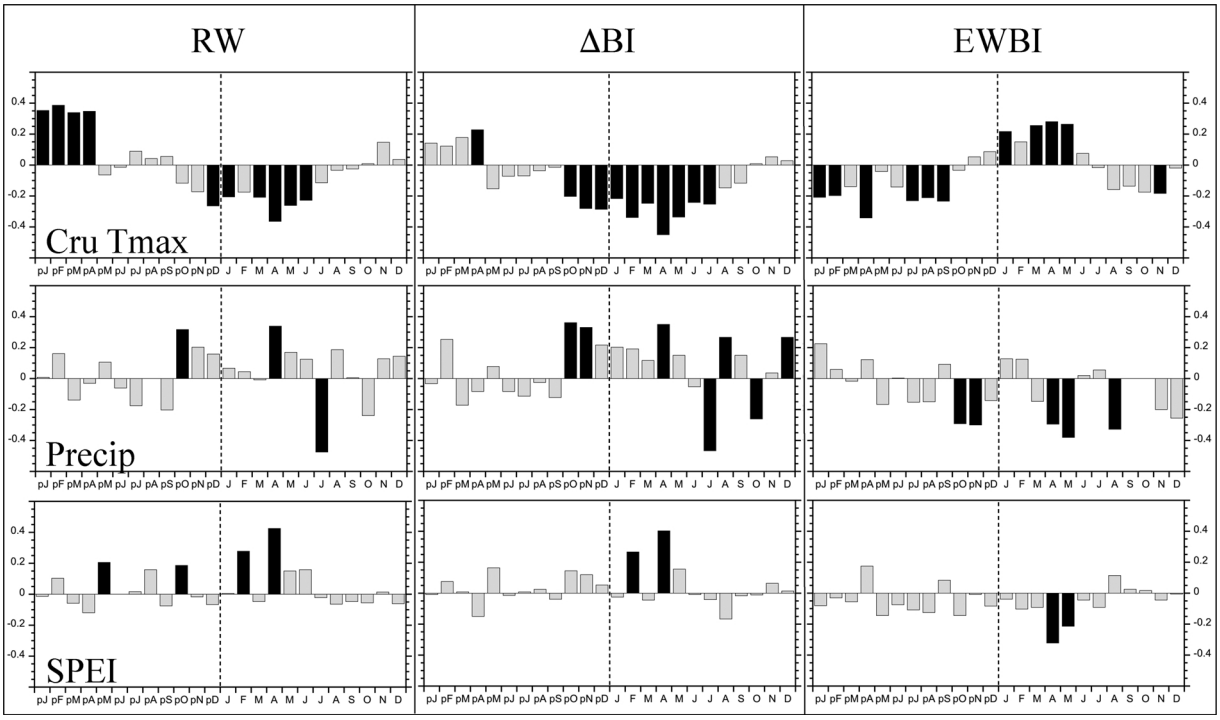

Fig. 7. The correlation response plots for RW (left), ΔBI (center) and EWBI (right) with maximum temperature (top row), precipitation (center) and SPEI (bottom). A 24-month response window is shown, with significant correlations shown in black. The vertical dashed lines mark the transition from prior year (left) to current year on the right.

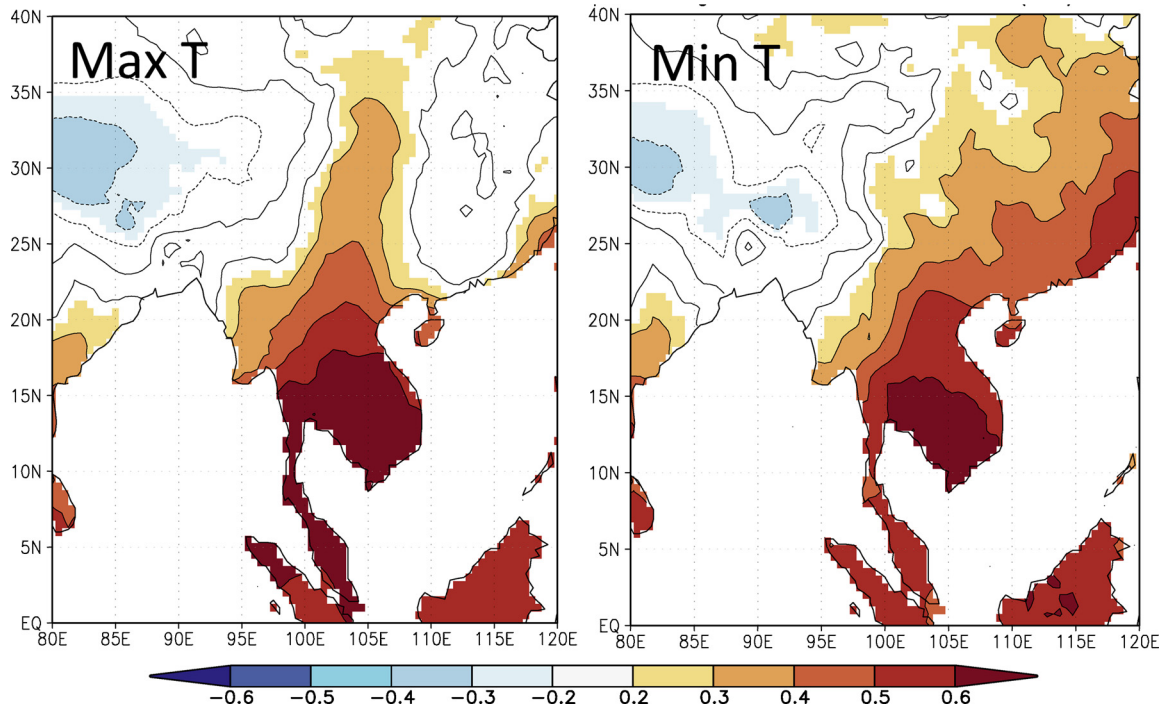

Fig. 8. EWBI against December to April maximum (left) and minimum (right) temperature from the CRU TS3.24.01 global temperature dataset for the span of 1902–2013. All data are first-differenced prior to correlation, and only areas of significant correlation are shown in color.

EARTH temperature series (Rhodes et al., 2013; Muller et al., 2013), and the standardized precipitation-evapotranspiration index or SPEI (Vicente-Serrano et al., 2013). We also used the Hadley Centre for Climate Prediction and Research HadSST3 global SST data.

3. Results and discussion

From the scanned images of our 29-core subset we produced indexed time series for RW, EWBI, LWBI, and ΔBI (Fig. 6). As noted above, we demonstrate in Fig. 5 that the essential RW-derived signal has not been lost with the reduction of samples between our 29-core RW indices and the original 71-core Buckley et al. (2017) QNFH record.

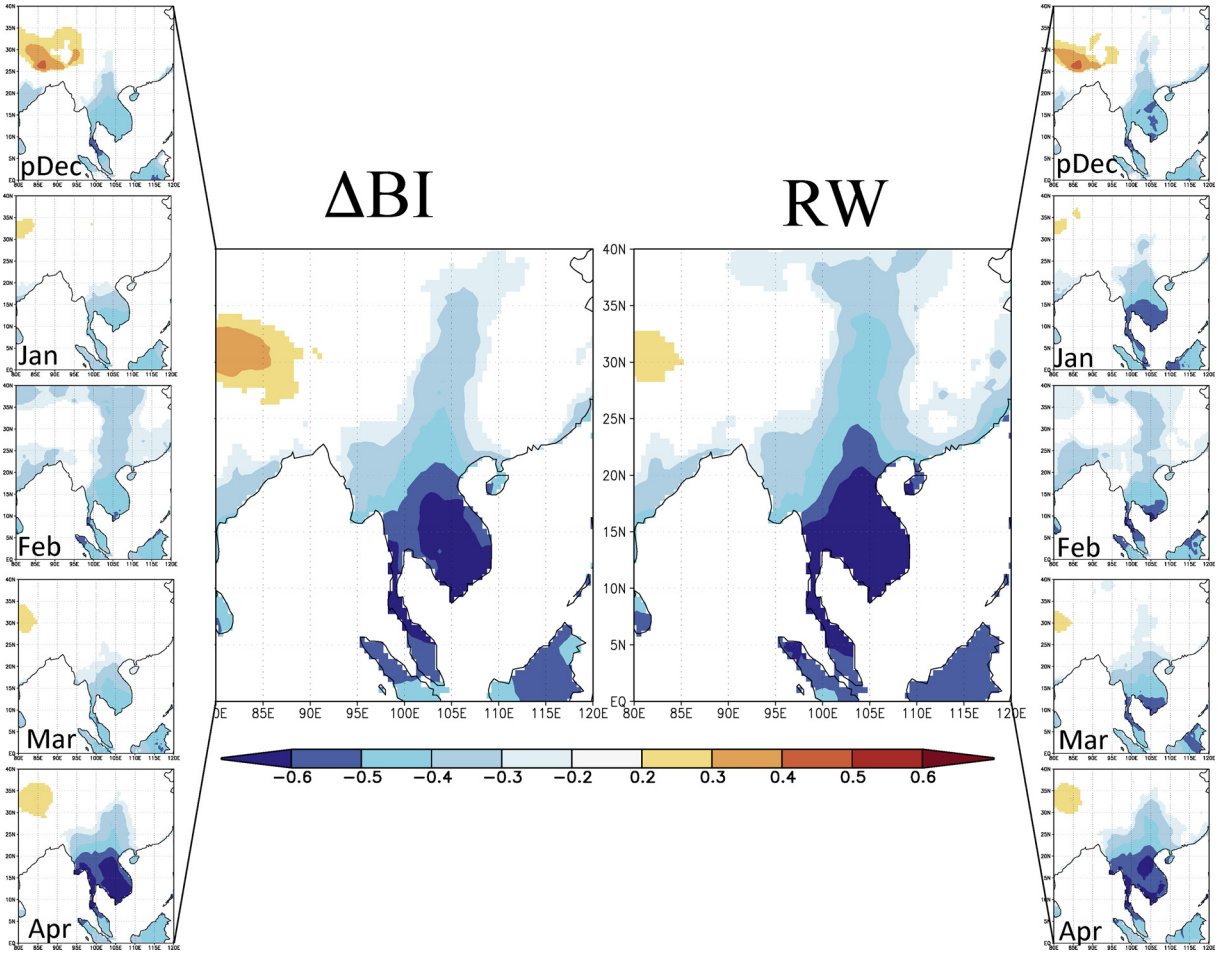

Fig. 9. Comparison of ΔBI (left) and RW (right) with maximum temperature for each month from prior December to April of the current year, from top to bottom, and for the entire 5-month season for the two centered plots.

The Rbar and EPS statistics (Fig. 6) reinforce that our smaller sample size adequately captures the overall variance of the larger population at least back to the year 1700 for the BI parameters, and back to 1600 for RW, based on the EPS threshold of 0.85 (Wigley et al., 1984). By comparison, the Buckley et al. (2017) version of this record extends back to the year 1347 and has an EPS value above 0.85 back to 1567, and it remains above 0.8 back to 1550.

3.1. Climate response of *Fokienia hodginsii* BI parameters

The response of all QNFH tree ring parameters to monthly maximum temperature, total precipitation and SPEI (Fig. 7) reinforces the importance of April as noted by Buckley et al. (2017) for RW. However, the strong, direct response to prior autumn rainfall for EWBI and ΔBI reinforces the idea that a pre-conditioning of the soil moisture by an increase in autumn rainfall is important for growth in the following year. From a density (BI) perspective, this suggests an increase in EW lignification (hence the inverse response shown in Fig. 7) during times of early season drought, which also corresponds to an overall reduction in RW. We also find that for EWBI the relationship with April SPEI after first differencing is strong and stable, while LWBI shows no significant response (LWBI response not shown). In fact, EWBI correlates significantly ($p < 0.05$) to temperature over the entire span of the dry season (Fig. 8), indicating that the warmer and therefore drier conditions are during the winter dry season (December–April), the more lignified the EW cells will be the following year. This has major implications for the role of xylem morphology in mitigating the effects of severe water and vapor pressure deficit (VPD) in order to protect plants from cavitation, as will be discussed below. The ΔBI exhibits the strongest correlation with prior autumn rainfall and prior November SPEI, and also rivals RW for its correlation with April SPEI (Fig. 7).

Buckley et al. (2017) found that the QNFH RW indices were directly correlated with spring hydroclimate over the central Vietnam region, a relationship strong enough to allow for a statistically stable reconstruction of the standardized precipitation-evapotranspiration index (SPEI, Vicente-Serrano et al., 2010) for the month of April. Although the QNFH index captured a similar ENSO-reflective correlation with sea surface temperature (SST) to *Fokienia* records from northern (Sano et al., 2009, 2012) and southern Vietnam (Buckley et al., 2010; 2014), respectively, a multi-decadal period of drought in the mid 18th century (1740–1770) was not as persistently expressed. These authors attributed an apparently dampened response to this epic period of drought, the so-called Strange Parallels Drought (Cook et al., 2010), to central Vietnam's autumn rainfall peak that is absent from the rest of Vietnam (Buckley et al., 2017; Li et al., 2015). These authors hypothesized that this regionally specific spike in rainfall for October and November serves to effectively dampen the effects of an annual dry period (November to April) that is more strongly expressed in northern and southern parts of Indochina. The proposed mechanism was the linkage between East Asian Winter Monsoon (EAWM) years that are modulated by strong El Niño years and their effect on the ensuing summer monsoon over central Vietnam (Chen et al., 2013). Hansen et al. (2017) reconstructed October-November rainfall from a Douglas fir record from a karst region of northern Vietnam and argued, as did Buckley et al. (2017) for QNFH, that autumn rainfall served to precondition trees before the long dry season.

Table 2
Split-period calibration and verification statistics for the winter temperature reconstruction shown in Fig. 10, and as described in the text. The top two panels show undifferenced and first differenced results for the calibration (verification) period of 1902–1959 (1960-2012). The bottom two panels reverse these two periods for the same statistics. Note the much higher statistics for RE and CE for the first differenced data for both periods, reflecting greater fidelity at higher frequency. The inclusion of DBI reduces the low-frequency variability of the predictor series, as discussed in the text.

Undifferenced Late Calibration (1960-2012) Verification (1902-1959)

Test	Score	T stat	Prob.	Score (v)	T-stat (v)	Prob. (v)
Equality of means	0.000	0.000	0.99571	−0.115	−1.281	0.19696
Cross products mean	0.194	2.736	0.00417	0.125	2.876	0.00283
Sign test	39 + 14-	3.297	0.00049	42 + 16-	3.283	0.00051
Pearson correlation	r = 0.607	5.449	0.00000	r = 0.619	5.903	0.00000
Robust correlation	r = 0.652	6.148	0.00000	r = 0.623	5.966	0.00000
Spearman correlation	r = 0.616	5.588	0.00000	r = 0.596	5.561	0.00000
Kendall Tau	t = 0.447	4.725	0.00000	t = 0.429	4.756	0.00000
Reduction of error	0.368			0.372		
Coefficient of efficiency	0.368			0.342		

First differenced Late Calibration (1960-2012) Verification (1902-1959)

Test	Score	T stat	Prob.	Score (v)	T-stat (v)	Prob. (v)
Equality of means	−0.005	−0.031	0.97344	0.016	0.118	0.90184
Cross products mean	0.589	2.822	0.00337	0.403	5.416	0.00000
Sign test	41 + 11-	4.022	0.00003	49 + 8-	5.298	0.00000
Pearson correlation	r = 0.747	7.937	0.00000	r = 0.753	8.485	0.00000
Robust correlation	r = 0.753	8.092	0.00000	r = 0.761	8.709	0.00000
Spearman correlation	r = 0.688	6.711	0.00000	r = 0.793	9.638	0.00000
Kendall Tau	t = 0.517	5.413	0.00000	t = 0.591	6.498	0.00000
Reduction of error	0.557			0.564		
Coefficient of efficiency	0.557			0.564		

Undifferenced Late Calibration (1960-2012) Verification (1902-1959)

Test	Score	T stat	Prob.	Score (v)	T-stat (v)	Prob. (v)
Equality of means	0.000	0.000	0.99571	−0.115	−1.281	0.19696
Cross products mean	0.194	2.736	0.00417	0.125	2.876	0.00283
Sign test	39 + 14-	3.297	0.00049	42 + 16-	3.283	0.00051
Pearson correlation	r = 0.607	5.449	0.00000	r = 0.619	5.903	0.00000
Robust correlation	r = 0.652	6.148	0.00000	r = 0.623	5.966	0.00000
Spearman correlation	r = 0.616	5.588	0.00000	r = 0.596	5.561	0.00000
Kendall Tau	t = 0.447	4.725	0.00000	t = 0.429	4.756	0.00000
Reduction of error	0.368			0.372		
Coefficient of efficiency	0.368			0.342		

First differenced Late Calibration (1960-2012) Verification (1902-1959)

Test	Score	T stat	Prob.	Score (v)	T-stat (v)	Prob. (v)
Equality of means	−0.005	−0.031	0.97344	0.016	0.118	0.90184
Cross products mean	0.589	2.822	0.00337	0.403	5.416	0.00000
Sign test	41 + 11-	4.022	0.00003	49 + 8-	5.298	0.00000
Pearson correlation	r = 0.747	7.937	0.00000	r = 0.753	8.485	0.00000
Robust correlation	r = 0.753	8.092	0.00000	r = 0.761	8.709	0.00000
Spearman correlation	r = 0.688	6.711	0.00000	r = 0.793	9.638	0.00000
Kendall Tau	t = 0.517	5.413	0.00000	t = 0.591	6.498	0.00000
Reduction of error	0.557			0.564		
Coefficient of efficiency	0.557			0.564		

3.2. BI and RW as predictors of climate

A further comparison of ΔBI and RW against maximum temperature across the span of the dry season from December to April (Fig. 9) shows the evolution of a response to atmospheric drought that culminates in a maximum inverse correlation with April, typically the month of highest maximum temperature across mainland Southeast Asia. This temperature maximum precedes the onset to the summer monsoon during what is the classic “shoulder season” of March-May, a time of transition from winter to summer monsoons. This is the period of reconstruction of hydroclimate from cypress records from northern (Sano et al., 2009) and southern Vietnam (Buckley et al., 2010). The relationship between RW/ΔBI and maximum temperature is sufficiently strong and stable to allow for a Principal Components based reconstruction of winter (Dec–Apr) maximum temperature based on current and prior year RW and ΔBI that explains nearly 37% of the variance of the instrumental data (Table 2). The actual and estimated values for split calibration periods, along with the full reconstruction (1550–2013), are shown in

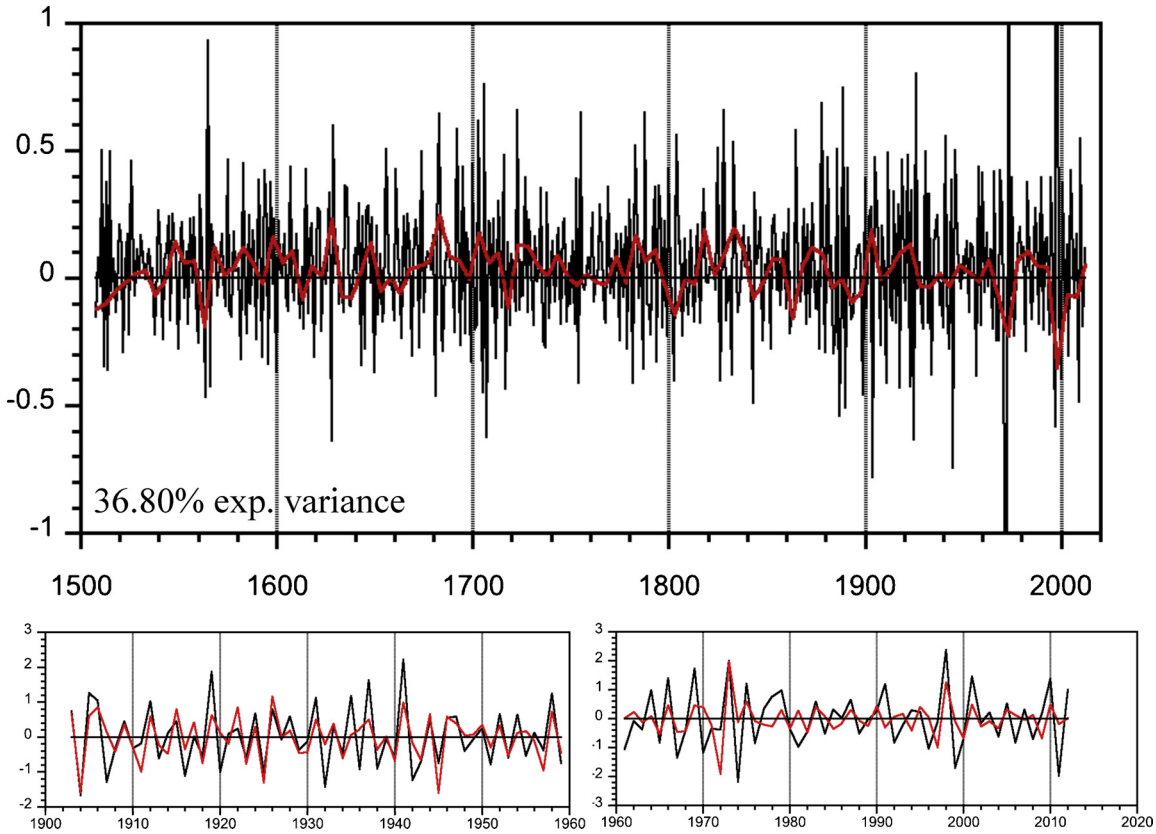

Fig. 10. Reconstruction (top) of Dec-Apr maximum temperature based on a PC regression model of RW and ΔBI for current and prior year. The calibration and verification plots (bottom) for 1910–1960 (left) and 1960–2013 (right). The reconstruction explains nearly 37% of the variance of the temperature data.

Fig. 10. This is the first reconstruction of the winter climate over Southeast Asia from tree rings, and offers a unique perspective on monsoon variability as will be discussed below. A further examination of the winter (Dec–Apr) climate response over land and sea (e.g., maximum air temperature and sea surface temperature, respectively, as shown in Fig. 11) for RW, ΔBI and EWBI, reinforces the importance of ENSO variability in the broader sense. This is consistent with prior research on this species over its entire range (Buckley et al., 2010, 2014, 2017; Sano et al., 2009, 2012).

3.3. The physiological basis for lignification of earlywood

The BI measurements we present in this paper represent time-varying degrees of lignification of tracheid cells in what we interpret to be a response to drought and heat stress. It is therefore important to understand the processes that exert control over the timing and magnitude of the lignification response, and how this may affect the function of xylem. Tracheid cells in the xylem of conifers create tiny conduits (typically 5–80 μm in diameter, and about 7 mm in length). Within the xylem, water flows in a continuous water column between the soil and the leaves through the open space within tracheid cells known as the lumen (Dixon and Joly, 1895; Hacke et al., 2004; Hacke, 2015). According to the cohesion-tension theory, as water evaporates from the leaves through the stomata, hydraulic tension pulls water up to the leaves from the soil through the xylem, maintaining the hydraulic conductance (Cochard et al., 2013). It is imperative for survival that this water column remains intact because if the tension becomes too great, such as under severe conditions of drought, the water column can be broken by an embolism as air is pulled into the xylem, thus cutting off the supply of water to the leaves (Zimmermann, 1983). Extensive embolisms caused by high evaporative demand and low soil water content may result in partial or complete tree mortality from cavitation, hence species have evolved to stave off cavitation through a variety of physiological responses (Larter et al., 2017). It is therefore possible that the reduction of lumen size through increased lignification of cell walls, as suggested in this study, constitutes an attempt to alleviate the risk of cavitation through a reduction in lumen diameter. Such reduction might be expected to reduce tension placed on the water column through high evaporative demand, and to further prevent the collapse or implosion of xylem cells due to negative pressure (Hacke et al., 2001).

The anatomical construction of conifer xylem plays an important role in the trade-offs between efficiency of water transport and hydraulic safety from cavitation. However, since it is leaf evapotranspiration that drives the movement of water through the xylem, future research should be aimed at better understanding the entire chain of processes between leaf and soil. The degree to which EWBI is driven by the empty space of the lumen rather than the tracheid walls requires further research. Since there is direct correlation between the cell wall thickness and the diameter of the lumen of each cell, this is something that can be measured directly, and is a logical follow up to the current study. We present a very preliminary result in Fig. 12 for a set of 10 rings of *Fokienia hodginsii* from southern Vietnam where we plot the ratio between cell wall thickness and lumen diameter (CWT/LD) for the entire ring against EWBI, and find that they are highly correlated ($r = 0.86$, $p = 0.001$). This result lends support to our interpretation of EWBI in this paper – that EWBI is reflecting actual density of the cells, and that the variability in EW density is linked to hydroclimate. A recent paper by Björklund et al. (2017) finds that for Northern Hemisphere conifers there is a distinct difference between the EW and LW density and their respective relationships to RW. For EW, an increase in density corresponds to a reduction of overall RW, while LW is positively correlated with RW. With regard to the current study, maximum temperature, during the lead up to the annual monsoon

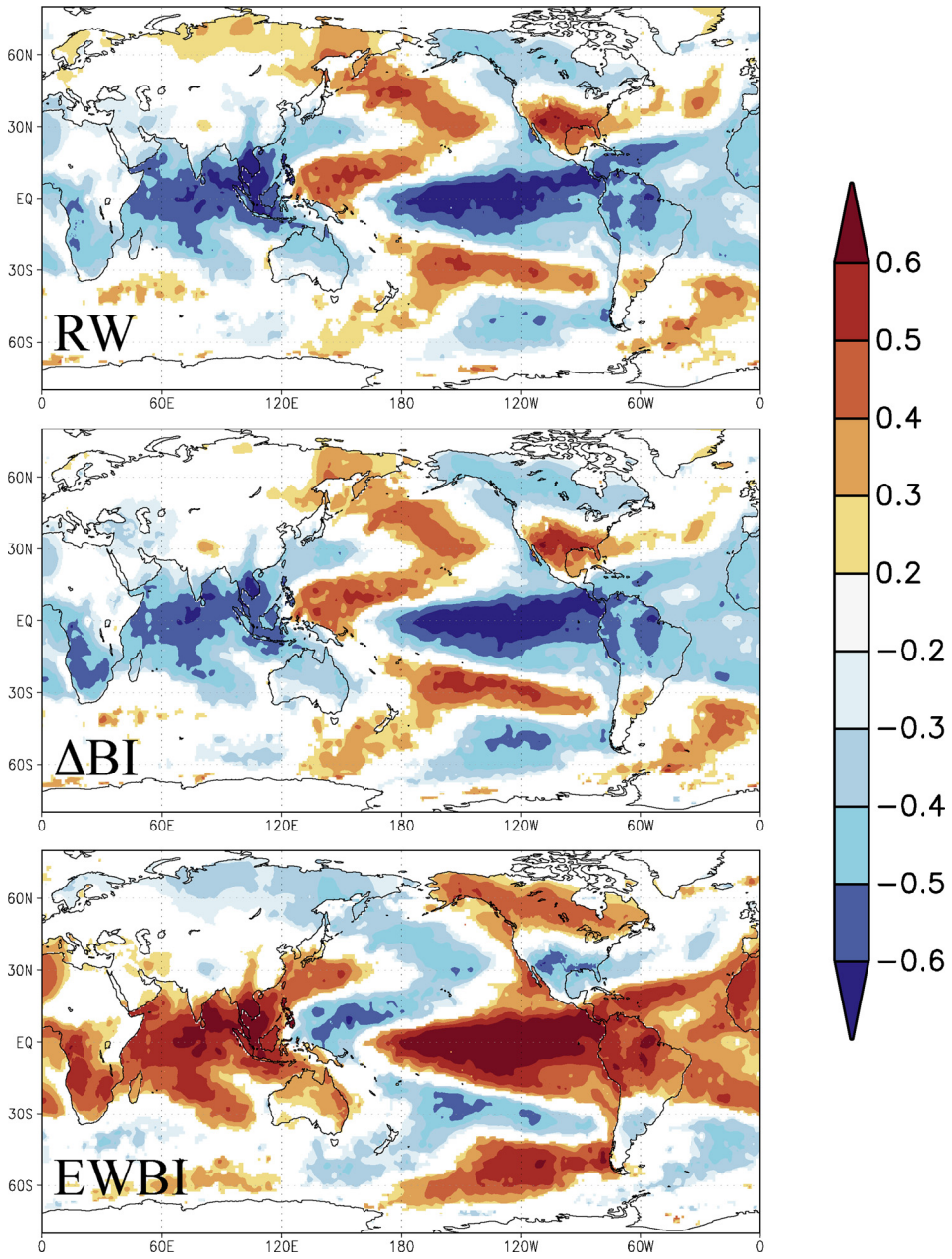

Fig. 11. Spatial correlation fields between RW (top), ΔBI (center) and EWBI (bottom) against maximum temperature over land from the CRU TS3.24.01 global dataset and sea surface temperature (SST) from the Hadley Centre for Climate Research for the December to April winter season. All data were first differenced prior to correlation over the period 1902–2013. Note the strong correlation over regions of related to ENSO, as noted by Buckley et al. (2010; 2014, 2017) for this species in Vietnam.

onset, is driving both an increase in EW density (i.e., a decrease in BI), as well as a reduction in annual RW.

4. Conclusions

We present here what is, to our knowledge, the first attempt at applying BI methodology to tropical trees, in this case on Vietnamese cypress trees growing in central Vietnam. A subset of 29 cores from 20 trees was selected from a previously published collection of 71 cores from 37 trees, and adequately captures the signal of the larger population. Comparisons between RW, EWBI, LWBI and ΔBI and their corresponding relationships with several climate parameters indicate that BI offers comparable strength of signal to RW, and may provide an independent variable to include for climate reconstruction. An important result of this study is a reconstruction of winter (December–April) maximum temperature for the Indochina Peninsula that explains nearly 37% of the variance of the original data. However for the study species (*Fokienia hodginsii*) at least, it is necessary to account for color changes that occur at the heartwood/sapwood boundary. For this study we used ΔBI, which results in an apparent loss of low frequency variability for our reconstruction (Fig. 10). We must therefore endeavor to find alternative methods for overcoming trend bias without sacrificing low frequency variability of our reconstructions. For the current study it is the variability of the EW that appears to be most strongly responsive to climate, rather than the more commonly used LW, and it is the severity of the annual dry season from December to April that triggers the BI response of the EW. We are interpreting the BI response as reflecting the true density of the EW cells, owing to the relationship between thickening of cell walls and reduction of lumen diameters in response to the threat of cavitation.

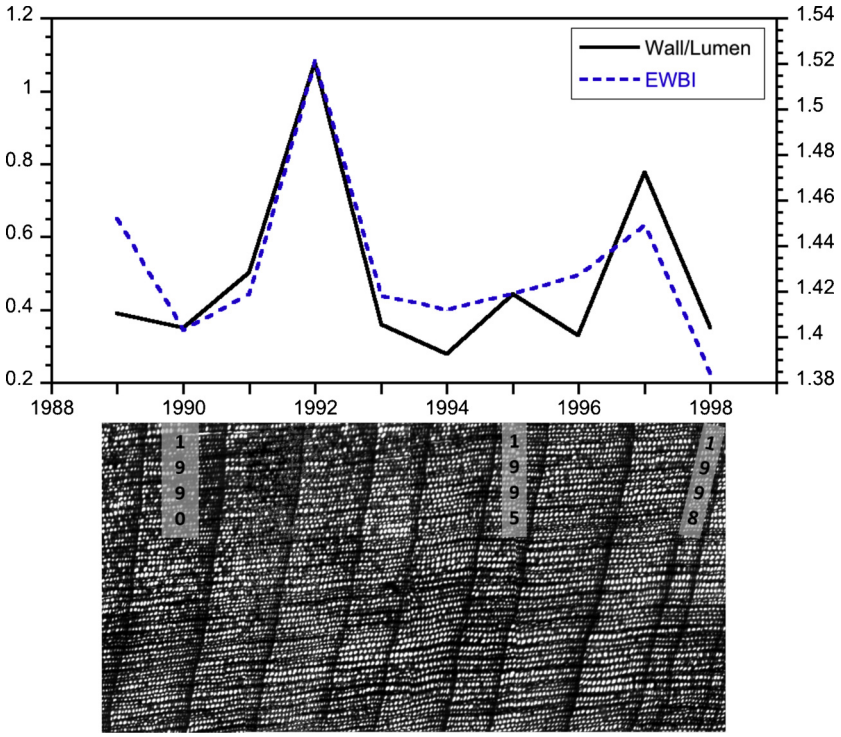

Fig. 12. Comparison of (top) EWBI (dashed line) with the ratio between cell wall thickness and lumen area for the entire ring (solid line) for a 10-ring segment of a *Fokienia hodginsii* core from central Vietnam, shown on the bottom.

We suggest with this paper that the lignification of EW cells during annual growth ring development might indicate a cavitation-avoidance response by reducing the size of lumens in order to maintain the integrity of the water column between the roots and the stomata. We have initiated research that aims to corroborate the results presented here, by direct measurements of cell wall thickness and lumen diameters from these same cores. It is clear from our study that BI relates to seasonal climate variability, and the response of EWBI in particular shows a very strong and coherent expression of ENSO-related variability across much of the planet (Fig. 11). Our database of cypress records extends from southern to northern Vietnam, and we are expanding into Laos on the western side of the Annamite Range. By combining RW and BI parameters there is great potential to produce the most highly robust tree-ring reconstructions of climate yet seen from the global tropics. We will continue to research the mechanisms of xylem genesis within the context of the ecophysiology of the species, and this should allow for mechanistic climate-growth models that are more accurate than the traditional empirically derived reconstructions.

Acknowledgements

This research was funded by the National Science Foundation of the USA research grants AGS 12-03818 and AGS 13-03976, with additional funding from the Lamont-Doherty Earth Observatory's Climate Center and Climate and Life initiatives. We are grateful to the forest rangers and staff at the various site locations from which we sampled throughout Vietnam. There are no conflicts of interest for any of the authors of this manuscript. All data generated from this project will be made available upon request. Lamont-Doherty Contribution No. 8207.

References

Björklund, J.A., Gunnarson, B.E., Seftigen, K., Esper, J., Linderholm, H.W., 2014. Blue intensity and density from northern Fennoscandian tree rings, exploring the potential to improve summer temperature reconstructions with earlywood information. Clim. Past 10, 877–885. http://dx.doi.org/10.5194/cp-10-877-2014.

Björklund, J., Gunnarson, B.E., Seftigen, K., Zhang, P., Linderholm, H.W., 2015. Using adjusted blue intensity data to attain high-quality summer temperature information: a case study from Central Scandinavia. Holocene 25 (3), 547–556.

Björklund, J., Seftigen, K., Schweingruber, F., Fonti, P., von Arx, G., Bryukhanova, M.V., Cuny, H.E., Carrer, M., Castagneri, D., Frank, D.C., 2017. Cell size and wall dimensions drive distinct variability of earlywood and latewood density in Northern hemisphere conifers. New Phytol. 216 (3), 728–740. http://dx.doi.org/10.1111/nph/14639.

Briffa, K.R., Osborn, T.J., Schweingruber, F.H., Jones, P.D., Shiyatov, S.G., Vaganov, E.A., 2002. Tree-ring width and density data around the Northern hemisphere: part 1, local and regional climate signals. Holocene 12 (6), 737–757.

Briffa, K.R., Melvin, T.M., 2011. A closer look at regional curve standardization of tree-ring records: justification of the need, a warning of some pitfalls, and suggested improvements in its application. In: Hughes, M.K., Swetnam, T.W., Diaz, H.F. (Eds.), Dendroclimatology. Springer, Netherlands, Dordrecht, pp. 113–145.

Buckley, B.M., Anchukaitis, K.J., Penny, D., Fletcher, R., Cook, E.R., Sano, M., Wichienkeeo, A., Minh, T.T., Hong, T.M., 2010. Climate as a contributing factor in the demise of Angkor, Cambodia. Proc. Natl. Acad. Sci. 107 (15), 6748–6752.

Buckley, B.M., Fletcher, R., Wang, S.Y.S., Zottoli, B., Pottier, C., 2014. Monsoon extremes and society over the past millennium on mainland Southeast Asia. Quat. Sci. Rev. 95, 1–19. http://dx.doi.org/10.1016/j.quascirev.2014.04.022.

Buckley, B.M., Stahle, D.K., Luu, H.T., Wang, S.Y.S., Nguyen, T.Q.T., Thomas, P., Le, C.N., Ton, T.M., 2017. Central Vietnam climate over the past five centuries from cypress tree rings. Clim. Dyn. 48 (11–12), 3707–3723.

Campbell, R., McCarroll, D., Loader, N.J., Grudd, H., Robertson, I., Jalkanen, R., 2007. Blue intensity in Pinus sylvestris tree-rings: developing a new palaeoclimate proxy. Holocene 17, 821–828. http://dx.doi.org/10.1177/0959683607080523.

Chen, W., Feng, J., Wu, R., 2013. Roles of ENSO and PDO in the link of the East Asian winter monsoon to the following summer monsoon. J. Clim. 26 (2), 622–635.

Cochard, H., et al., 2013. Methods for measuring plant vulnerability to cavitation: a critical review. J. Exp. Bot. 64 (15), 4779–4791.

Cook, E.R., 1985. A Time Series Analysis Approach to Tree-Ring Standardization. Ph.D. Dissertation. University of Arizona, Tucson p. 171.

Cook, E.R., Kairiukstis, L., 1990. Methods of Dendrochronology. Springer, New York.

Cook, E.R., Peters, K., 1997. Calculating unbiased tree-ring indices for the study of climatic and environmental change. Holocene 7 (3), 361–370.

Cook, E.R., Anchukaitis, K.J., Buckley, B.M., D'Arrigo, R.D., Jacoby, G.C., Wright, W.E., 2010. Asian monsoon failure and megadrought during the last millennium. Science 328 (5977), 486–548.

D'Arrigo, R., Frank, D., Jacoby, G., Pederson, N., 2001. Spatial response to major volcanic events in or about AD 536, 934 and 1258: frost rings and other dendrochronological evidence from Mongolia and northern Siberia: comment on RB Stothers,'Volcanic dry fogs, climate cooling, and plague pandemics in Europe and the Middle East'(climatic change, 42, 1999). Clim. Change 49 (1), 239–246.

D'Arrigo, R., Buckley, B.M., Kaplan, S., Woollett, J., 2003. Interannual to multidecadal modes of Labrador climate variability inferred from tree rings. Clim. Dyn. 20, 219–228. http://dx.doi.org/10.1007/s00382-002-0275-3.

D'Arrigo, R., Wilson, R., Anchukaitis, K.J., 2013. Volcanic cooling signal in tree ring

temperature records for the past millennium. J. Geophy. Res.: Atmos. 118 (16), 9000–9010.
Dixon, H.H., Joly, J., 1895. On the ascent of sap. Phil. Trans. R. Soc. B Biol. Sci. 186.
Dolgova, E., 2016. June–September temperature reconstruction in the Northern Caucasus based on blue intensity data. Dendrochronologia 39, 17–23.
Esper, J., Büntgen, U., Luterbacher, J., Krusic, P., 2013. Testing the hypothesis of post-volcanic missing rings in temperature sensitive dendrochronological data. Dendrochronologia 31, 216–222.
Esper, J., Schneider, L., Smerdon, J.E., Schöne, B.R., Büntgen, U., 2015. Signals and memory in tree-ring width and density data. Dendrochronologia 35, 62–70.
Filion, L., Payette, S., Gauthier, L., Boutin, Y., 1986. Light rings in subarctic conifers as a dendrochronological tool. Quat. Res. 26 (2), 272–279.
Fritts, H.C., 1976. Tree Rings and Climate.
Fukazawa, K., 1992. Ultraviolet microscopy. In: Lin, S.Y., Dence, C.W. (Eds.), Methods in Lignin Chemistry. Springer, Berlin, Heidelberg, pp. 110–121.
Gindl, W., 1999. Climatic Significance of Light Rings in Timberline spruce, Picea Abies, Austrian Alps. Arctic, Antarctic, and Alpine Research. pp. 242–246.
Gindl, W., Grabner, M., Wimmer, R., 2000. The influence of temperature on latewood lignin content in treeline Norway spruce compared with maximum density and ring width. Trees Struct. Funct. 14, 409–414.
Hacke, U.G. (Ed.), 2015. Functional and Ecologycal Xylem Anatomy. Springer International Publishing, Cham, Switzerland.
Hacke, U.G., Sperry, J.S., Pockman, W.T., Davis, S.D., McCulloh, K.A., 2001. Trends in wood density and structure are linked to prevention of xylem implosion by negative pressure. Oecologia 126, 457–461. http://dx.doi.org/10.1007/s004420100628.
Hacke, U.G., Sperry, J.S., Pittermann, J., 2004. Analysis of circular bordered pit function II. Gymnosperm tracheids with torus-margo pit membranes. Am. J. Bot. 91 (3), 386–400.
Hansen, K.G., Buckley, B.M., Zottoli, B., D'Arrigo, R.D., Van Truong, V., Nguyen, D.T., Nguyen, H.X., 2017. Discrete seasonal hydroclimate reconstructions over northern Vietnam for the past three and a half centuries. Clim. Change 145 (1-2), 177–188.
Hoffmann, W.A., Marchin, R.M., Abit, P., Lau, O.L., 2011. Hydraulic failure and tree dieback are associated with high wood density in a temperate forest under extreme drought. Glob. Change Biol. 17 (8), 2731–2742.
Jacoby, G.C., Workman, K.W., D'Arrigo, R.D., 1999. Laki eruption of 1783, tree rings, and disaster for northwest Alaska inuit. Quat. Sci. Rev. 18 (12), 1365–1371.
Lange, P.W., 1954. The distribution of lignin in the cell wall of normal and reaction wood from spruce and a few hardwoods. Sven. Papperstidn 57, 525–532.
Larsson, L.-Å, 2016. CDendro & CooRecorder Program Package for Tree Ring Measurements and Crossdating of the Data, Version 8.1.1. http://www.cybis.se/forfun/dendro.
Larter, M., Pfautsch, S., Domec, J.-C., Trueba, S., Nagalingum, N., Delzon, S., 2017. Aridity drove the evolution of extreme embolism resistance and the radiation of conifer genus Callitris. New Phytol. 215, 97–112. http://dx.doi.org/10.1111/nph.14545.
Li, R., Wang, S.Y., Gillies, R.R., Buckley, B.M., Truong, L.H., Cho, C., 2015. Decadal oscillation of autumn precipitation in Central Vietnam modulated by the East Pacific–North Pacific (EP–NP) teleconnection. Environ. Res. Lett. 10 (2), 024008.
Melvin, T.M., Briffa, K.R., 2008. A "signal-free" approach to dendroclimatic standardisation. Dendrochronologia 26 (2), 71–86.
Melvin, T.M., Briffa, K.R., 2014. CRUST: software for the implementation of regional chronology standardisation: part 1. Signal-free RCS. Dendrochronologia 32 (1), 7–20.
Melvin, T.M., Briffa, K.R., Nicolussi, K., Grabner, M., 2007. Time-varying-response smoothing. Dendrochronologia 25, 65–69. http://dx.doi.org/10.1016/j.dendro.2007.01.004.
Mork, E., 1960. The relationship between temperature, leader growth, and growth and lignification of annual rings in Spruce. Meddelelser fra det Norske Skogsforsoksvesen 56, 227–261.
Muller, R.A., Curry, J., Groom, D., Jacobsen, R., Perlmutter, S., Rohde, R., Rosenfeld, A., Wickham, C., Wurtele, J., 2013. Decadal variations in the global atmospheric land temperatures. J. Geophys. Res. Atmos. 118 (11), 5280–5286.
Rhode, R., Muller, R.A., Jacobsen, R., Muller, E., Perlmutter, S., Rosenfeld, A., Wurtele, J., Groom, D., Wickham, C., 2013. A new estimate of the average earth surface land temperature spanning 1753-2011. Geoinform. Geostat. 2013 (1), 1. http://dx.doi.org/10.4172/2327-4581.1000101.
Rydval, M., Larsson, L.-Å., McGlynn, L., Gunnarson, B.E., Loader, N.J., Young, G.H.F., Wilson, R., 2014. Blue intensity for dendroclimatology: should we have the blues? Experiments from Scotland. Dendrochronologia 32, 191–204. http://dx.doi.org/10.1016/j.dendro.2014.04.003.
Rydval, M., Gunnarson, B.E., Loader, N.J., Cook, E.R., Druckenbrod, D.L., Wilson, R., 2017a. Spatial reconstruction of Scottish summer temperatures from tree rings. Int. J. Climatol. 7 (3), 1540–1556. http://dx.doi.org/10.1002/joc.4796.
Rydval, M., Loader, N.J., Gunnarson, B.E., Druckenbrod, D.L., Linderholm, H.W., Moreton, S.G., Wood, C.V., Wilson, R., 2017b. Reconstructing 800 years of summer temperatures in Scotland from tree rings. Clim. Dyn. 1–24.
Sano, M., Buckley, B.M., Sweda, T., 2009. Tree-ring based hydroclimate reconstruction over northern Vietnam from Fokienia hodginsii: eighteenth century mega-drought and tropical Pacific influence. Clim. Dyn. 33 (2–3), 331.
Sano, M., Xu, C., Nakatsuka, T., 2012. A 300-year Vietnam hydroclimate and ENSO variability record reconstructed from tree ring $\delta^{18}O$. J. Geophys. Res. Atmos. 117 (D12).
Schweingruber, F.H., 2012. Tree Rings: Basics and Applications of Dendrochronology. Springer Science & Business Media 266 pp.
Szeicz, J.M., 1996. White spruce light rings in northwestern Canada. Arctic Alpine Res. 184–189.
Starheim, C.C., Smith, D.J., Prowse, T.D., 2013. Dendrohydroclimate reconstructions of july–august runoff for two nival-regime rivers in west central British Columbia. Hydrol. Process. 27 (3), 405–420.
Trouet, V., Van Oldenborgh, G.J., 2013. KNMI climate explorer: a web-based research tool for high-resolution paleoclimatology. Tree Ring Res. 69 (1), 3–13.
Harris, I.C., Jones, P.D., 2017. UEACRU; CRU TS3.24.01: Climatic Research Unit (CRU) Time-Series (TS) Version 3.24.01 of High Resolution Gridded Data of Month-by-month Variation in Climate (Jan. 1901- Dec. 2015). Centre for Environmental Data Analysis 03/2017.
Vicente-Serrano, S.M., Beguería, S., López-Moreno, J.I., 2010. A multiscalar drought index sensitive to global warming: the standardized precipitation evapotranspiration index. J. Clim. 23 (7), 1696–1718.
Vicente-Serrano, S.M., Gouveia, C., Camarero, J.J., Beguería, S., Trigo, R., López-Moreno, J.I., Azorín-Molina, C., Pasho, E., Lorenzo-Lacruz, J., Revuelto, J., Morán-Tejeda, E., 2013. Response of vegetation to drought time-scales across global land biomes. Proc. Natl. Acad. Sci. 110 (1), 52–57.
Vincent, J.F., 1999. From cellulose to cell. J. Exp. Biol. 202 (23), 3263–3268.
Waito, Justin, Conciatori, France, Tardif, Jacques C., 2013. Frost rings and white early-wood rings in *Picea mariana* trees from the boreal plains, central Canada. IAWA J. 34 (1), 71–87.
Wang, S.Y.S., Promchote, P., Truong, L.H., Buckley, B., Li, R., Gillies, R., Trung, N.T.Q., Guan, B., Minh, T.T., 2014. Changes in the autumn precipitation and tropical cyclone activity over Central Vietnam and its East Sea. Vietnam J. Earth Sci. 36 (4), 489–496.
Wigley, T.M., Briffa, K.R., Jones, P.D., 1984. On the average value of correlated time series, with applications in dendroclimatology and hydrometeorology. J. Climate Appl. Meteorol. 23 (2), 201–213.
Wilson, R.J.S., Luckman, B.H., 2003. Dendroclimatic reconstruction of maximum summer temperatures from upper tree-line sites in interior British Columbia. Holocene 13 (6), 853–863.
Wilson, R., Rao, R., Rydval, M., Wood, C., Larsson, L.Å., Luckman, B.H., 2014. Blue intensity for dendroclimatology: the BC blues: a case study from British Columbia, Canada. Holocene 24 (11), 1428–1438.
Wilson, R., Anchukaitis, K., Briffa, K., Büntgen, U., Cook, E., Arrigo, R.D.', Davi, N., Esper, J., Frank, D., Gunnarson, B., Hegerl, G., Klesse, S., Krusic, P., Linderholm, H., Myglan, V., Peng, Z., Rydval, M., Schneider, L., Schurer, A., Wiles, G., Zorita, E., 2016. Last millennium northern hemisphere summer temperatures from tree rings: part I: the long term context. Quat. Sci. Rev. 134, 1–18.
Wilson, R., Wilson, D., Rydval, M., Crone, A., Büntgen, U., Clark, S., Ehmer, J., Forbes, E., Fuentes, M., Gunnarson, B.E., Linderholm, H.W., 2017a. Facilitating tree-ring dating of historic conifer timbers using blue intensity. J. Archaeol. Sci. 78, 99–111.
Wilson, R., D'Arrigo, R., Andreu-Hayles, L., Oelkers, R., Wiles, G., Anchukaitis, K., Davi, N., 2017b. Blue Intensity based experiments for reconstructing North Pacific temperatures along the Gulf of Alaska. EGU General Assembly Conference Abstracts Vol. 19http://dx.doi.org/10.5194/cp-2017-26. (p. 7716).
Xiao, S.C., Xiao, H.L., Peng, X.M., Tian, Q.Y., 2014. Daily and seasonal stem radial activity of Populus euphratica and its association with hydroclimatic factors in the lower reaches of China's Heihe river basin. Environ. Earth Sci. 72 (2), 609–621.
Yan, L., Li, W., Yang, J., Zhu, Q., 2004. Direct visualization of straw cell walls by AFM. Macromol. Biosci. 4 (2), 112–118.
Yatagai, A., Kamiguchi, K., Arakawa, O., Hamada, A., Yasutomi, N., Kitoh, A., 2012. APHRODITE: constructing a long-term daily gridded precipitation dataset for Asia based on a dense network of rain gauges. Bull. Am. Meteorol. Soc. 93 (9), 1401–1415.
Zimmermann, M.H., 1983. Xylem Structure and the Ascent of Sap. Available at:. Springer Berlin Heidelberg, Berlin, Heidelberg. http://link.springer.com/10.1007/978-3-662-22627-8.